Noname manuscript No.
(will be inserted by the editor)

D.T. Steinmoeller · S.J.D. D'Alessio · F.J. Poulin

Prograde and Retrograde Flow Past Cylindrical Obstacles on a β-plane

Received: date / Accepted: date

Abstract The problem of viscous prograde (eastward) and retrograde (westward) flow past a cylindrical obstacle on a β-plane is considered. The barotropic vorticity equation is solved using a numerical method that combines finite difference and spectral methods. A modified version of the β-plane approximation is proposed to avoid computational difficulties associated with the traditional β-plane approximation. Numerical results are presented and discussed for flow past a circular cylinder at selected Reynolds numbers (Re) and non-dimensional β-parameters ($\hat{\beta}$) as well as for flow past an elliptic cylinder of a fixed aspect ratio ($r = 0.2$) at inclination angles of $\pm 15°, 90°$ and selected Re and $\hat{\beta}$. In prograde flows, it is found that the β-effect acts to suppress boundary-layer separation and to excite a standing Rossby lee wavetrain, as observed in previous works. In retrograde flows, the boundary-layer separation region is elongated and westward propagating Rossby waves are excited.

Keywords GFD · beta-plane · Rossby waves · separation · boundary-layers · viscous · vorticity · cylinders · prograde · retrograde · flow

D.T. Steinmoeller
Department of Applied Mathematics, University of Waterloo, 200 University Ave. W, Waterloo, ON, N2L 3G1, CANADA
Tel.: 1-519-888-4567 x32588
Fax: 1-519-746-4319
E-mail: dsteinmo@math.uwaterloo.ca

S.J.D. D'Alessio
Department of Applied Mathematics, University of Waterloo, 200 University Ave. W, Waterloo, ON, N2L 3G1, CANADA

F.J. Poulin
Department of Applied Mathematics, University of Waterloo, 200 University Ave. W, Waterloo, ON, N2L 3G1, CANADA

1 Introduction

While the problem of flow past cylindrical obstacles in non-rotating fluids is a classical and well documented one, its rotating counterpart that accounts for the effects of differential rotation has only recently received attention. The numerical study of [16] applied the paradigm of flow past a circular cylinder on a β-plane to better understand the separation of the Gulf Stream at Cape Hatteras and the interaction between the Antarctic Circumpolar Current and various topographical features. Their numerical method utilized a finite difference scheme on a channel of finite width with a piece-wise constant approximation for the cylindrical obstacle. In agreement with earlier works, they found that the β-effect inhibits boundary-layer separation and causes a stagnant flow region to form upstream of the cylinder. They also found that for large Re ($Re > 200$) and moderate $\hat{\beta}$ ($\hat{\beta} \sim 10 - 100$) Rossby waves break in the turbulent wake of the cylinder causing meandering separated zonal jets to form at the shoulders of the cylinder. This observation is coincident with the assertion of [14] that rotating turbulent flow has a tendency to organize into a series of alternating zonal jets separated by the Rhines scale $L_R = (U/\beta)^{1/2}$. They observed that these zonal jets initially form due to boundary-layer separation, and extend quite far downstream depending on how far the Rossby wave-breaking region extended.

Earlier works such as [13], [8], and [18] studied eastward flow past cylinders on a beta-plane using models that were both laminar and inviscid. [18] solved the steady model equations for flow past circular cylinders analytically in an attempt to model eastward flow past an island, while [13] solved the unsteady equations for flow past a symmetric Joukowski aerofoil numerically. The study of [8] was an analytic study that also considered Ekman friction. In each study, they observed a standing Rossby wavetrain downstream of the cylinder in prograde flows. [13] and [8] also observed a blocked or stagnant flow region upstream of the cylinder if the β-effect was sufficiently strong. [3] carried out an experimental study where they observed that boundary-layer separation was suppressed in eastward flows and enhanced in westward flows.

The main goal of the present study is to extend the works in the literature to include flow past elliptic cylindrical obstacles as well as both prograde (eastward) and retrograde (westward) laminar flows using a β-plane approximation. Here, we use the convention that the terms "prograde" and "retrograde" are related to the direction of the Earth's rotation. The flow configuration is illustrated in Figure 1 for the case of uniform westward (retrograde) flow past an elliptic cylinder having an aspect ratio of $r = b/a$ inclined at an angle of η with the positive x-axis.

The numerical method employed, which is fully explained in [15], represents a combination of spectral and finite difference methods. A boundary-layer coordinate is introduced to accurately resolve the viscous boundary-layer and a conformal mapping is used to address the geometry of the cylindrical obstacle, thus eliminating the need for a piece-wise constant approximation as used in [16]. Although the numerical method is best suited to capture the early flow development following an abrupt startup, we will demonstrate that it also works well for moderate times. Focusing on this

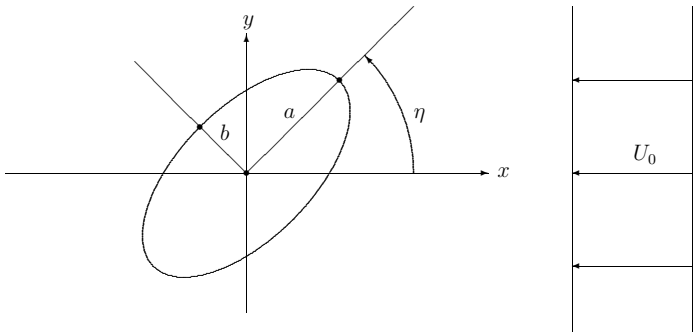

Fig. 1 The flow configuration for uniform westward flow.

time regime reinforces our underlying assumptions that the flow remains laminar and two-dimensional. Lastly, a modified form of the traditional β-plane approximation is proposed and implemented in our numerical scheme to avoid computational difficulties that may arise when the traditional β-plane approximation is applied to a large or unbounded domain.

The paper is organized as follows. The governing equations and non-dimensional parameters are stated in section 2. Following this, a modified β-plane approximation is introduced and discussed in section 3. Then, in section 4 the numerical method is briefly discussed. The results of our simulations are presented and discussed in section 5. Finally, concluding remarks are given in section 6.

2 Governing Equations

We assume that the dynamics are governed by the barotropic vorticity equation

$$\frac{\partial \zeta}{\partial t} + \mathbf{u} \cdot \nabla (\zeta + f) = \nu \nabla^2 \zeta, \tag{1}$$

where ζ is the relative vorticity, $\mathbf{u}$ is the fluid velocity, ν is the kinematic eddy viscosity of the fluid, and $f = 2\Omega \sin\theta \approx f_0 + \beta y$ is the usual β-plane approximation to the Coriolis parameter which captures the meridional variation of the Coriolis parameter from a central latitude θ_0, where $\theta = \theta_0 + y/R$ with R denoting the radius of the Earth.

The coefficient $\beta = (2\Omega \cos\theta_0)/R$ is commonly interpreted as the meridional gradient of the vertical component of planetary vorticity (divided by R). A simpler, and perhaps more satisfying interpretation, is that β is equal to the horizontal component of planetary vorticity $2\Omega \cos\theta_0$ (divided by R) that arises from the vector form of the planetary vorticity tilting term in the three-dimensional vorticity equation. A direct correspondence between the planetary vorticity tilting term and the β-term in the barotropic vorticity equation is established in [17].

Since we are assuming that the flow is two-dimensional and incompressible for all times of interest, it is useful to express the velocity in terms of a

streamfunction, ψ, where $\mathbf{u} = \mathbf{k} \times \nabla\psi$. Choosing the length scale to be the semi-major axis length a (or the cylinder radius for the case of a circular cross section) and the velocity scale to be the zonal uniform far-field velocity U_0, the vorticity equation can be rewritten in terms of the non-dimensional variables $(\tilde{x}, \tilde{y}) = (x, y)/a$, $\tilde{\mathbf{u}} = \mathbf{u}/U_0$, $\tilde{\zeta} = a\zeta/U_0$, $\tilde{\psi} = \psi/(aU_0)$, $\tilde{t} = U_0 t/a$. After dropping tildes, the non-dimensional vorticity equation becomes

$$\frac{\partial \zeta}{\partial t} + J(\psi, \zeta) + \hat{\beta}\frac{\partial \psi}{\partial x} = \frac{2}{Re}\nabla^2\zeta, \tag{2}$$

where

$$J(a, b) \equiv \frac{\partial a}{\partial x}\frac{\partial b}{\partial y} - \frac{\partial a}{\partial y}\frac{\partial b}{\partial x} ,$$

is the Jacobian operator, $Re = 2aU_0/\nu$ is the familiar Reynolds number, and $\hat{\beta} = a^2\beta/U_0$ is the non-dimensional β-parameter. The non-dimensional β-parameter is often interpreted as an inverse Rossby number (see [4]), characterizing the dominance of rotational effects. In [16], they demonstrate that $\hat{\beta}$ is also a measure of the extent to which fluid parcels are confined meridionally. In particular, for $\hat{\beta} < 1$ the fluid parcels are largely free to propagate in the meridional direction, while for $\hat{\beta} \geq 1$, the β-effect acts as a strong restoring force, causing the fluid parcels to propagate as Rossby waves.

Equation (2) is to be solved in conjunction with the streamfunction equation given by

$$\zeta = \nabla^2\psi, \tag{3}$$

to form a coupled closed system for the unknown flow variables (ψ, ζ).

3 The Modified β-plane

The traditional β-plane approximation $f = f_0 + \beta y$ can be problematic for large or unbounded domains. Hence, we propose an alternate β-plane approximation given by

$$f = f_0 + \beta\left[\alpha R \tanh\left(\frac{y}{\alpha R}\right)\right] , \tag{4}$$

where α is a free parameter, and R is the radius of the Earth. For small y, it is clear that (4) will recover the standard β-plane approximation to order $O((y/R)^3)$. Equation (4), on the other hand, limits f to the interval:

$$2\Omega(\sin\theta_0 - \alpha\cos\theta_0) < f < 2\Omega(\sin\theta_0 + \alpha\cos\theta_0) ,$$

where Ω is the Earth's rotation rate. The extent to which (4) behaves linearly is controlled by the parameter α. Using equation (4) enables us localize the linear variation of the Coriolis parameter, and thus allows us to solve the problem on a much larger domain.

We remark to the reader that the main purpose of this modified approximation is to make the problem computationally simpler, and not to improve on the accuracy of the traditional β-plane approximation. By artificially forcing f to tend to a constant for large y, we allow the barotropic

vorticity equation to asymptotically take the form of the familiar non-rotating two-dimensional vorticity equation that satisfies simple uniform far-field flow conditions. Appropriate far-field conditions for the traditional β-plane approximation are investigated in [13].

Equation (4) can easily be incorporated into the governing equations by simply replacing β in the dimensional barotropic vorticity equation (1) with $\beta \mathrm{sech}^2(y/\alpha R)$. In non-dimensional form, this modification yields

$$\frac{\partial \zeta}{\partial t} + J(\psi, \zeta) + \hat{\beta} \mathrm{sech}^2 \left(\frac{y}{\hat{\alpha}} \right) \frac{\partial \psi}{\partial x} = \frac{2}{Re} \nabla^2 \zeta, \tag{5}$$

where the dimensionless parameter $\hat{\alpha} = \alpha(R/a)$ now replaces α.

The physical impact of using the modified β-plane approximation is that Rossby waves that are generated will be confined to a finite region centered about $y = 0$ having a meridional extent which scales like $\hat{\alpha}$. Thus, including equation (4) has the effect of creating a waveguide centered about the central latitude which traps Rossby waves. Since $\hat{\alpha}$ is an arbitrary parameter, it can be chosen to be large enough so that the trapped Rossby waves do not compromise our numerical results for small to moderate times t.

As a final note we wish to comment on the steady-state far-field solution to the barotropic vorticity equation (2) for the case of uniform eastward flow. Adopting the linearization first proposed by [11], we have shown that the asymptotic solution can be expressed in polar coordinates (r, ϕ) as follows

$$\zeta \sim \left(C \sqrt{\frac{2\pi}{Rer}} \exp(-\frac{Re}{4} r[1 - \cos\phi]) - \hat{\beta} r \right) \sin\phi \, ,$$

for large r where C is an undetermined constant. The solution reveals that apart from $\phi = \pi$ and a narrow wake region concentrated about $\phi = 0$, the vorticity grows without bound in accordance with the usual β-plane approximation. By replacing $\hat{\beta}$ with $\hat{\beta}\mathrm{sech}^2(r \sin\phi/\hat{\alpha})$ this undesired growth will be suppressed.

4 Numerical Method

The governing equations are rewritten in terms of the modified polar coordinates (ξ, ϕ) which are related to the Cartesian coordinates (x, y) through a mapping of the form $x + iy = H(\xi + i\phi)$ where for a circular cylinder

$$H(\xi + i\phi) = \exp(\xi + i\phi) \, ,$$

while for an elliptic cylinder

$$H(\xi + i\phi) = \cosh[(\xi + \xi_0) + i(\phi + \eta)] \, ,$$

with $\tanh \xi_0 = r$. This choice of coordinates is better suited to the geometry and makes the prescription of boundary conditions more natural since the

cylinder surface is mapped to the line $\xi = 0$ and the infinite region exterior to the cylinder is mapped to the semi-infinite rectangular strip

$$\xi \geq 0 \ , \ -\pi \leq \phi \leq \pi \ .$$

Another important feature associated with the mapping is that the radial grid-spacing grows exponentially as we depart from the cylinder's surface. This feature is numerically beneficial because we can resolve the no-slip boundary-layer with a much smaller number of grid points than if we were to use a uniformly-spaced grid.

We choose to impulsively start the flow from rest at $t = 0$ since doing so allows the structure of the no-slip boundary-layer to be taken into account initially. We introduce the boundary-layer coordinate $z = \xi/\lambda$ with $\lambda = \sqrt{8t/Re}$. This change of variables allows the physical grid to expand with the boundary-layer as time progresses and thus helps to better resolve the thin no-slip boundary-layer for small times. The governing equations are then reformulated in terms of the boundary-layer coordinate z, along with the scaled streamfunction $\Psi = \psi/\lambda$ and vorticity $\omega = \lambda\zeta$. It is worth noting that once the boundary-layer thickens appreciably, the switch can be made back to the physical coordinate ξ.

The numerical technique utilized is a combination of a spectral and finite-difference scheme. The technique is based on the method employed by [1] in their study of unsteady uniform flow past a translating and rotating circular cylinder. The method has proven to be an efficient approach for solving two-dimensional flow problems past cylindrical bodies governed by the Navier-Stokes equations expressed in a streamfunction – vorticity formulation as demonstrated in [1] and [2].

The underlying idea is to expand the flow variables in a truncated Fourier series and then to solve the resulting partial differential equations for the Fourier coefficients using finite difference methods. The equations for the vorticity Fourier coefficients, after being discretized in time using a Crank-Nicolson scheme, are time-stepped by iteration. Spatial derivatives with respect to the boundary-layer coordinate z, are discretized using second-order centered differences. Determining the surface vorticity involves implementing global constraints taking the form of integral conditions which are exact and are derived in [6]. Marching schemes are used to update the streamfunction Fourier coefficients at each iteration, as done in [5]. Full details of the numerical solution procedure can be found in [15].

5 Numerical Results

To confirm numerical convergence, numerous numerical experiments were carried out with different grids and time steps. From these experiments we have found the scheme to be both flexible and robust for physical parameter values of $Re \sim 100 - 2000$ and $\hat{\beta} \leq 10$. From our numerical experiments the following values for the computational parameters were adopted for typical runs: $z_\infty = 10$, $N = 51$, $L = 401$, $\hat{\alpha} = 25$ and $\varepsilon = 10^{-6}$. Here, z_∞ denotes the outer boundary approximating infinity, N refers to the number of terms

retained in the truncated Fourier series, L is the number of equally spaced grid points used to discretize the boundary-layer coordinate z, and ε represents the convergence criterion that was applied to successive iterates of the surface vorticity. For results presented in this paper with $\hat{\beta} = 10$, the number of grid points in z was increased to $L = 801$ and the number of terms in the truncated Fourier series was increased to $N = 101$. This change was made because the former choice of parameters appears to overstate the influence of Rossby wave breaking in the flow field.

Small initial time steps of $\Delta t = 10^{-4}$ were used to advance past the abrupt startup. With the passage of time Δt was steadily increased to $\Delta t = 0.01$ and then held constant for $t \geq 1$. No stability difficulties were encountered with the choice of grid and parameters listed above. Lastly, comparisons with the numerical works of [7] and [5] for the non-rotating or f-plane case ($\hat{\beta} = 0$) were carried out to validate our numerical results. Comparisons of drag and lift coefficients with these studies were in good agreement. Since these aforementioned studies both solved the steady equations, comparisons could only be carried out at low Reynolds numbers ($Re < 100$).

We next present and discuss output from our numerical simulations for selected parameter values.

5.1 Prograde Flow Past a Circular Cylinder

We first consider prograde (west-to-east) uniform flow past a circular cylinder. The motivation here is to remind the reader of the dynamics of the classical problem of unsteady viscous flow past a circular cylinder at moderately large Reynolds numbers ($Re \sim 200 - 1000$), and also to illustrate the impact that differential rotation, i.e. the β-effect, has on the flow. Numerical results have been obtained for $\hat{\beta} = 0, 1, 10$. The non-zero values of $\hat{\beta}$ are based on typical oceanic velocities of $U \sim 10^{-1}$ ms^{-1} and typical beta-parameters of $\beta \sim 10^{-11}$ m^{-1}s^{-1} for obstacles having length scales of L $\sim$ 100 km and 300 km.

Figure 2 displays snapshots of the flow field for the case $\hat{\beta} = 0$ and $Re = 200$ at various times. These plots reveal that boundary-layer separation sets in well before $t = 2$ and the separation bubble initially grows in length before eventually settling down. At $t = 8$ and $t = 14$ a symmetric pair of vortices are visible illustrating the recirculating flow that occurs in the separation region. We have observed that these vortices remain stable for all times t considered. However, they do become unstable to small-amplitude perturbations as we will later demonstrate.

With $\hat{\beta} = 1$ and $Re = 200$, shown in Figure 3, the β-effect is clearly visible when contrasted with Figure 2. The downstream separation region is noticeably smaller, as demonstrated analytically by [10], this is because the β-effect suppresses boundary-layer separation by shifting the region of adverse pressure gradient towards the rear stagnation point. A standing Rossby wavetrain is also visible in the flow field downstream of the cylinder at times $t = 8$ and $t = 14$. Wavetrains of this nature were also observed in the numerical studies of [16] and [13], the analytical works of [18] and [8], as well

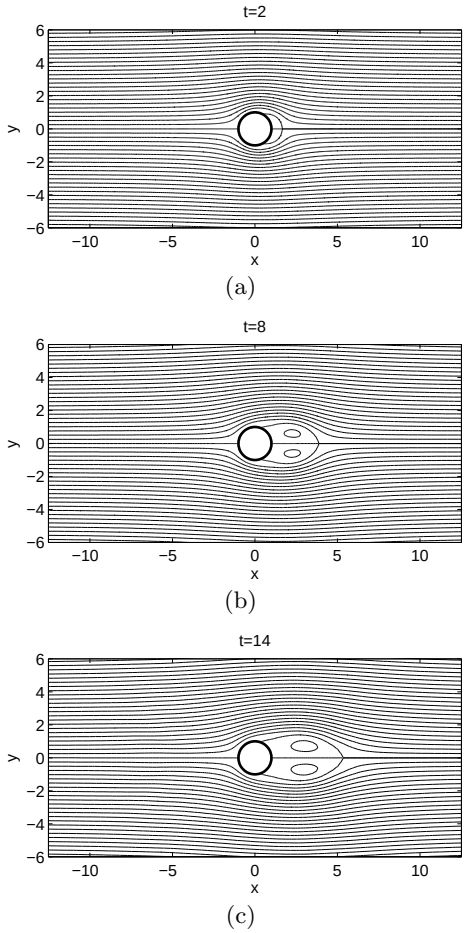

Fig. 2 Streamlines of prograde flow past a circular cylinder for the parameters $Re = 200$, $\hat{\beta} = 0$.

as in the experimental study of [3]. According to inviscid linear wave theory, stationary Rossby waves in a prograde flow have a dimensionless wavelength of $\lambda = 2\pi/\hat{\beta}^{1/2}$. In Figure 3, $\hat{\beta} = 1$ so the standing Rossby waves should have a dimensionless wavelength of $\lambda \approx 2\pi$. Our results appear to confirm this prediction.

We next increase the Reynolds number to $Re = 1000$. The effect of a significantly larger Reynolds number is that it weakens the dissipation in the simulation by decreasing the effective viscosity, thereby increasing the role of nonlinear advection of vorticity. Plotted in Figures 4, 5, 6 are the cases having $\hat{\beta} = 0, 1, 10$, respectively. The changes observed in increasing $\hat{\beta}$ from $\hat{\beta} = 0$ to $\hat{\beta} = 1$ are similar to the corresponding figures for $Re = 200$. The primary difference is that the standing Rossby waves are more clearly

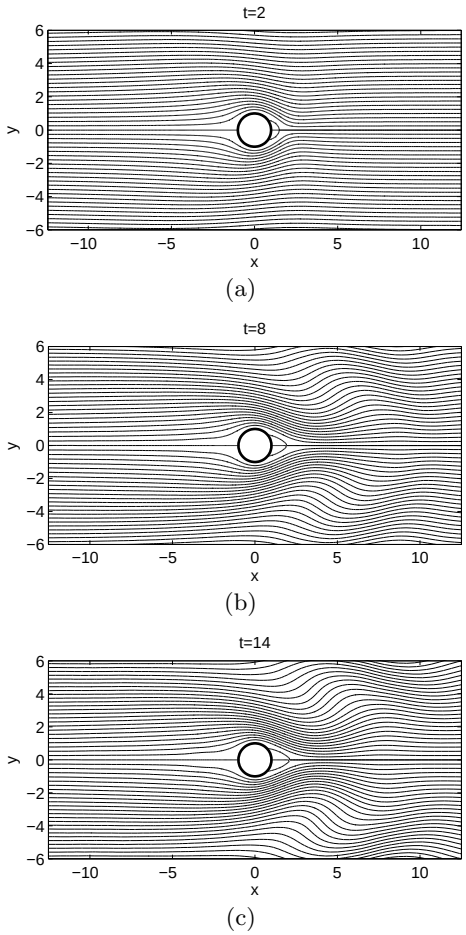

Fig. 3 Streamlines of prograde flow past a circular cylinder for the parameters $Re = 200$, $\hat{\beta} = 1$.

visible in the the flow field, both downstream and upstream. This is because decreasing the effective dissipation amounts to less dampening of the Rossby waves. In agreement with the studies of [13] and [8], a near stagnant flow region is present on the upstream side of the cylinder.

Further increasing $\hat{\beta}$ to $\hat{\beta} = 10$ shows a flow field dominated by Rossby wave activity in Figure 6. Here, the stationary Rossby waves have a much shorter dimensionless wavelength of $\lambda \approx 2$. Linear wave theory also suggests that any excited wave having a wavelength that is longer than that of the standing waves should propagate to the *west*, while any wave having a wavelength that is shorter than that of the standing waves should propagate to the *east*. This theoretical prediction explains why Rossby waves are seen throughout the flow field. Another important feature of the $\hat{\beta} = 10$ case is

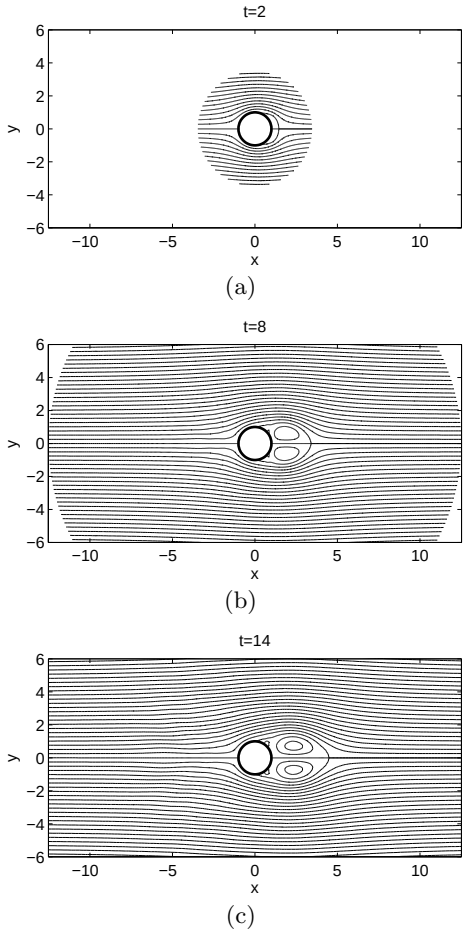

Fig. 4 Streamlines of prograde flow past a circular cylinder for the parameters $Re = 1000$, $\hat{\beta} = 0$.

that breaking Rossby waves are present. A signature of wave-breaking is the small vortices that are clearly visible away from the cylinder by $t = 8$ and $t = 14$. Although it may not be obvious from examing Figure 6, when the flow is animated these vortices are seen to originate from the crests of steepening Rossby waves. [16] also observed Rossby wave breaking in their simulations for $\hat{\beta} \geq 10$. The suppressing nature of the β-effect on boundary-layer separation is very strong in this case and thus results in a tiny separation bubble on the cylinder's lee side. This separation region is flanked by two regions of very densely-packed streamlines which can be interpreted as western boundary currents arising from western intensification. [16] observed in their simulations with $\hat{\beta} \sim 10 - 100$ that these western boundary currents separate entirely from the cylinder becoming zonal jets which extend quite

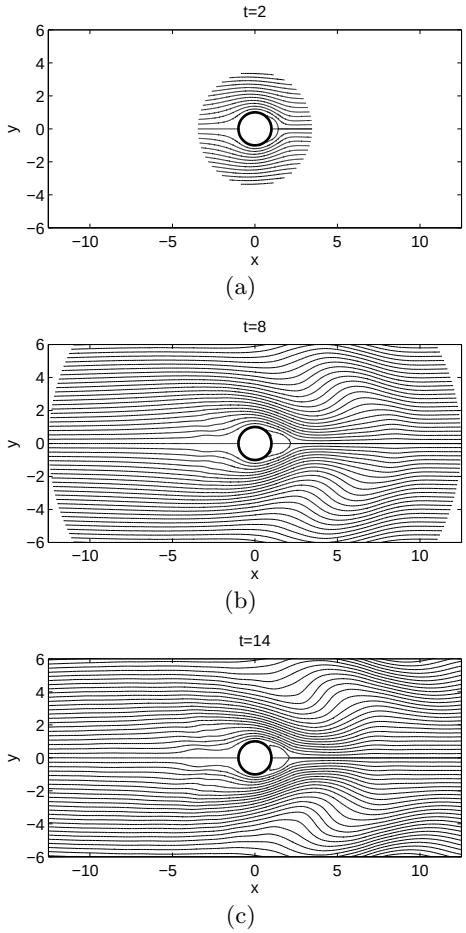

Fig. 5 Streamlines of prograde flow past a circular cylinder for the parameters $Re = 1000$, $\hat{\beta} = 1$.

far downstream and are maintained by breaking Rossby waves originating from inside the cylinder's wake. In our results, the cylinder's wake remains small and the two western boundary currents follow along the tiny separation bubble where they appear to meet at $y = 0$. They do, however, extend a considerable distance downstream as a single zonal jet due to breaking Rossby waves away from the cylinder's wake. The process of mean flow generation by breaking Rossby waves is one that is well documented, especially in the Earth's atmosphere (see for example [12] or [9]).

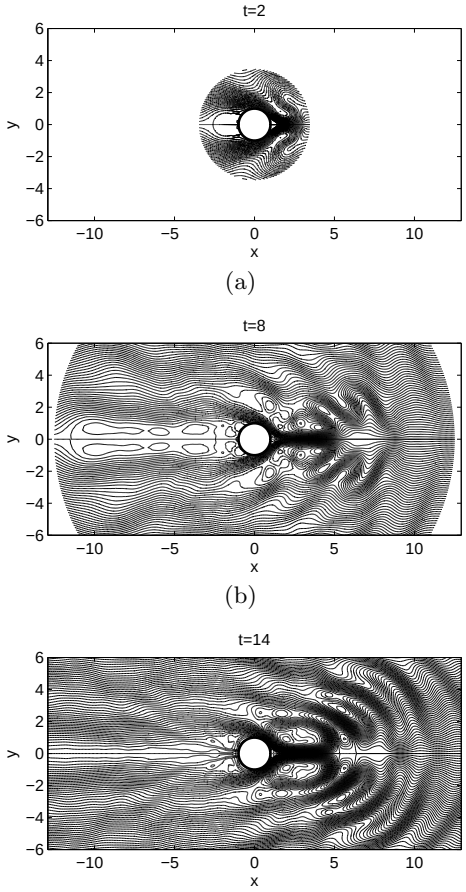

Fig. 6 Streamlines of prograde flow past a circular cylinder for the parameters $Re = 1000$, $\hat{\beta} = 10$.

Figure 7 compares surface vorticity (ζ_0) distributions for different $\hat{\beta}$ values for the case $Re = 1000$ at time $t = 14$. The surface vorticity is given by

$$\zeta_0 = \left(\frac{\partial v_\theta}{\partial \xi} \right)_0 , \tag{6}$$

and is of fundamental importance because a necessary condition for boundary-layer separation is that ζ_0 changes sign. A change in the sign of ζ_0 corresponds to a direction change in the tangential component of the velocity, v_θ, near the surface, i.e. a flow reversal.

A striking observation in these surface vorticity distributions is in the extent to which the variations in ζ_0 are excited when $\hat{\beta} = 10$. The case where

$\hat{\beta} = 1$, however, appears to have similar magnitudes and gradients to that in the non-rotating case when $\hat{\beta} = 0$. This discrepancy can be explained by the increased western intensification near the surface of the cylinder when $\hat{\beta} = 10$. In the case where $\hat{\beta} = 1$, western intensification only has a small effect, and thus we can expect the surface vorticity to be similar to the case where there is no differential rotation ($\hat{\beta} = 0$). The only visible difference between the $\hat{\beta} = 1$ and $\hat{\beta} = 0$ cases is a shift in the distributions due to the change in locations of the separation points.

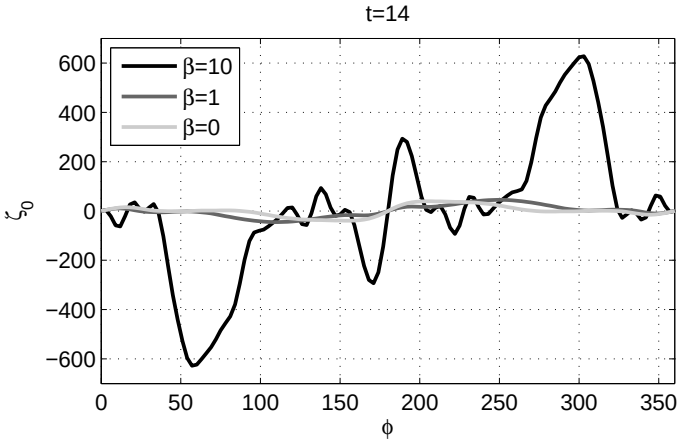

Fig. 7 Distributions of the surface vorticity ζ_0 at $t = 14$ for the parameters $Re = 1000$ and $\hat{\beta} = 0, 1, 10$.

The flow patterns presented thus far have been symmetric with respect to the x-axis. We expect that for moderately large Reynolds numbers the flow should become unstable to small perturbations and then evolve into the famous Von Kármán vortex street for the non-rotating case. This is precisely what we observe in Figure 8 for $Re = 1000$, $\hat{\beta} = 0$ which displays vortices alternately forming on the top and bottom halves of the cylinder backside and ultimately shedding and being swept downstream. A disturbance was introduced in this simulation by adding small amplitude random noise to the Fourier coefficients of the flow variables (ψ, ζ) at time $t = 1$.

A very different pattern occurred when a similar disturbance was added to the case having $Re = 1000$, $\hat{\beta} = 1$ shown in Figure 9. At times $t = 2$ and $t = 3$ we see a vortex forming and an asymmetric flow field beginning to develop. As expected the growth of the vortex is suppressed and remains attached and at $t = 5$ we see that the attached vortex appears to have moved along the cylinder surface in the clockwise direction and another vortex has formed near the front of the cylinder. In addition, on the northern side of the separation region tightly packed streamlines are evident which suggests that an intensified current is forming. Shortly after $t = 5$ our method became numerically unstable.

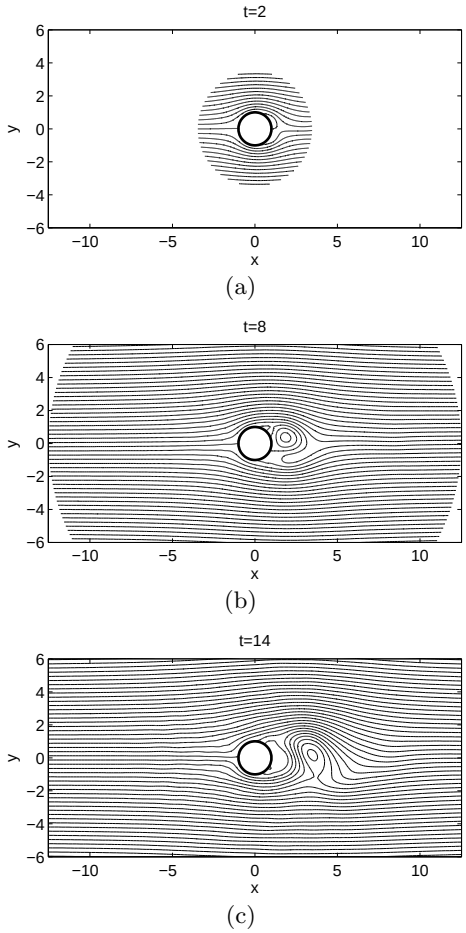

Fig. 8 Streamlines of perturbed prograde flow past a circular cylinder for the parameters $Re = 1000$, $\hat{\beta} = 0$.

5.2 Retrograde Flow Past a Circular Cylinder

We now turn to retrograde (east-to-west) uniform flow past a circular cylinder. The motivation behind these results is to illustrate the differences between prograde and retrograde flow for moderately large Reynolds numbers and $\hat{\beta} = 1, 10$. Of course with $\hat{\beta} = 0$ retrograde and prograde flows will be mirror images of each other about the y-axis.

Figure 10 shows streamline plots of retrograde flow past a circular cylinder for the case $Re = 200$ and $\hat{\beta} = 1$ at selected times. The most striking difference between prograde and retrograde flow is in the structure of the separation region. An elongated separation bubble is seen to result from retrograde flow, contrary to the shortened separation bubble observed with prograde

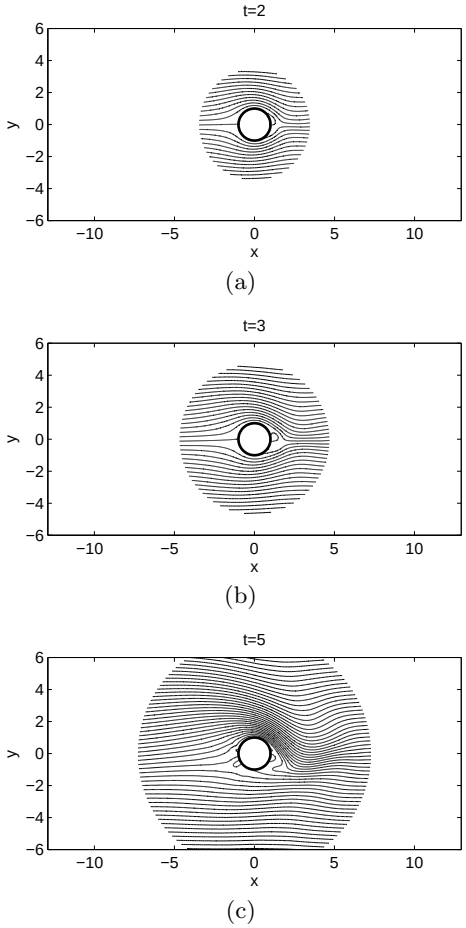

(a) (b) (c)

Fig. 9 Streamlines of perturbed prograde flow past a circular cylinder for the parameters $Re = 1000$, $\hat{\beta} = 1$.

flow. The stretched separation region weakens the recirculating flow taking place inside of it. [10] predicted analytically that the β-effect should have no influence on structure of the boundary-layer in retrograde flow. Comparing the points of separation in Figures 2 and 10, this analytical result appears to be consistent with our numerical findings. In addition, the experiments of [3] suggest that separation is enhanced in westward flows. Our results agree with these observations since the flow separation regions are clearly larger when $\hat{\beta} > 0$ than when $\hat{\beta} = 0$. Another key difference between prograde and retrograde flow is in the behavior of Rossby waves which are barely noticeable in Figure 10; they are only evident near the x-axis upstream of the cylinder where the oncoming flow is retarded. Even though the linear wave theory predicts that in retrograde flow the Rossby wave crests must always travel

to the west, the zonal group speed may be in either direction depending on $\hat{\beta}$ and on the wavenumber. This explains why it possible to observe Rossby waves on the upstream side of our obstacle in retrograde flows: The flow "feels" the upstream influence of the cylindrical obstacle.

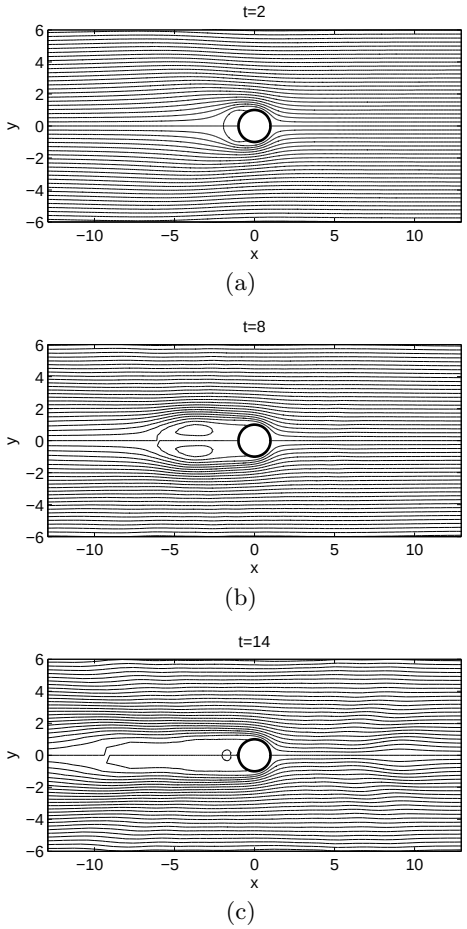

Fig. 10 Streamlines of retrograde flow past a circular cylinder for the parameters $Re = 200$, $\hat{\beta} = 1$.

Figure 11 illustrates retrograde flow for $Re = 1000$ again with $\hat{\beta} = 1$. Increasing the Reynolds number appears to have the same effect as in the prograde case, namely that the recirculation vortices are strengthened and the Rossby waves are less dampened by viscosity making them slightly more evident in the flow field. When $\hat{\beta}$ is increased to $\hat{\beta} = 10$ and the Reynolds number is fixed at $Re = 1000$ the flow field is is not dramatically different

as when $\hat{\beta} = 1$. As shown in Figure 12, the main difference is that strong flow intensification is initiated near the points of separation and continues downstream as a pair of separated zonal jets. Above and below these jets, travelling Rossby waves are clearly evident. Contrary to the prograde flow case with the same set of physical parameters (Figure 6), these inertial jets remain separated because the separation region is elongated by the β-effect, and not constricted to a tiny recirculation bubble. Another key difference is that there appears to be no Rossby wave breaking here, even though the β-effect is quite strong. Rossby waves are largely unevident in the flow field until $t = 8$, but they do become more apparent by $t = 14$. As observed in the case of prograde flow, retrograde flow also remains symmetrical about the x-axis. To break the symmetry we introduce a small disturbance into the flow field at $t = 1$ as previously explained. Figure 13 shows the perturbed flow for the case with $Re = 1000$ and $\hat{\beta} = 1$. Contrasting this with the corresponding unperturbed case portrayed in Figure 11, we see that the only difference appears to be in the wake at $t = 14$. In fact, at $t = 8$ there appears to be very little asymmetry.

5.3 Prograde Flow Past an Elliptic Cylinder

We now consider flow past elliptic cylinders on the β-plane. To prescribe this flow we need to specify the inclination, η, and the aspect ratio of the ellipse, r, in addition to Re and $\hat{\beta}$. In an attempt to reduce the parameter space to a manageable dimension, we consider a slender ellipse having $r = 0.2$, and vary the inclination. When $\eta \neq 0, 90^\circ$ the flow is inherently asymmetric and obtaining numerical solutions was more difficult for larger $\hat{\beta}$ values. For this reason we focused on $\hat{\beta} \leq 1$.

We begin with the symmetric case having $\eta = 90^\circ$, $Re = 1000$ and $\hat{\beta} = 1$ displayed in Figure 14. We have chosen to not show the non-rotating ($\hat{\beta} = 0$) case with $\eta = 90^\circ$, since the results are analogous to the results when the obstacle was circular. However, the case of $\hat{\beta} = 1$ is interesting because it illustrates how the β-effect behaves when the obstacle is more slender. The primary difference between the results here and those with a circular obstacle can be attributed to the rapid change in curvature near the tips of the cylinder. With $\hat{\beta} = 1$ the suppressing nature of the β-effect is even stronger than that witnessed in Figure 5 for the circular cylinder. A stagnant region is also seen to form and grow in front of the cylinder. Rossby waves are clearly visible downstream of the cylinder.

We next turn to the asymmetric case of prograde flow past an elliptic cylinder inclined at an angle of 15° ($\eta = -15^\circ$) relative to the free stream with $Re = 1000$ and $\hat{\beta} = 0, 0.75$ illustrated in Figures 15, 16, respectively. With $\hat{\beta} = 0$, Figure 15 represents a classical depiction of vortex shedding whereby vortices regularly form behind the cylinder and then shed and get carried downstream. As they propagate downstream they weaken due to viscosity. The situation is quite different when $\hat{\beta} \neq 0$ as shown in Figure 16. First we note that Rossby waves are not discernible in this plot since their

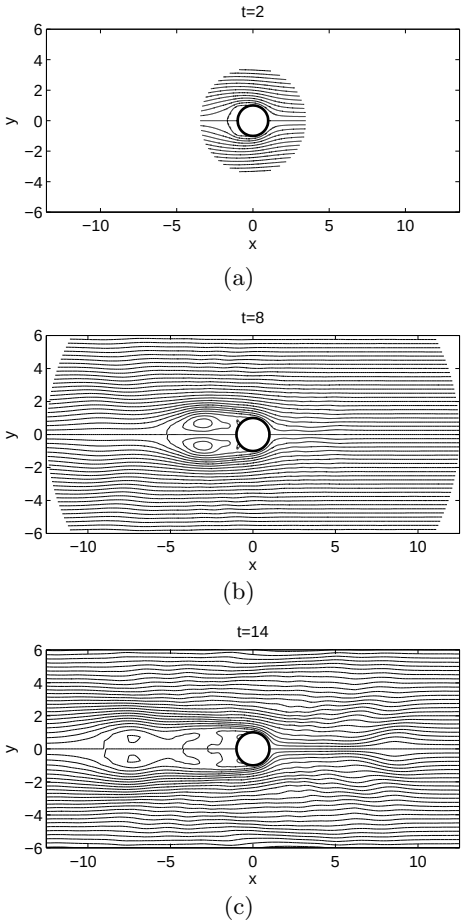

Fig. 11 Streamlines of retrograde flow past a circular cylinder for the parameters $Re = 1000$, $\hat{\beta} = 1$.

wavelengths are comparable to the dimension of the domain. As previously reported for the case of the circular cylinder, the β-effect suppresses vortex shedding to a small separation region near the cylinder's trailing edge. The shed vortices appear to be swept around the trailing edge in a clockwise direction, rather than in the expected downstream direction. Although it is not evident from Figure 16, our simulations indicate that as these vortices propagate southward they expand and gain strength in accordance with conservation of potential vorticity. Also, the northern edge of the separation region and the cylinder are flanked by a region of tightly packed streamlines indicating a western boundary current has formed, but the flow is relatively stagnant south of the cylinder. This flow behavior is similar to that observed for perturbed prograde flow past a circular cylinder. The case when $\hat{\beta} = 0.25$

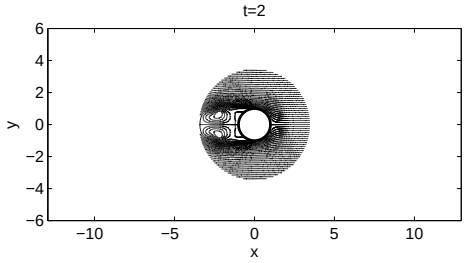

(a)

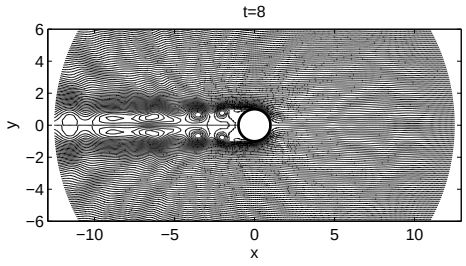

(b)

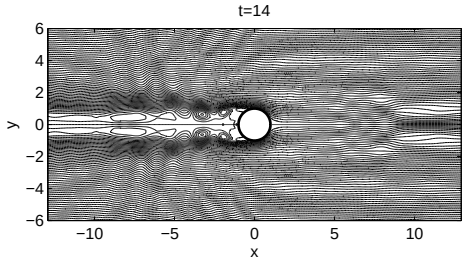

(c)

Fig. 12 Streamlines of retrograde flow past a circular cylinder for the parameters $Re = 1000$, $\hat{\beta} = 10$.

(not shown) was also considered. When increasing $\hat{\beta}$ from 0.25 to 0.75, the only discernible qualitative difference between the two cases was that vortex shedding occured sooner in the latter case.

5.4 Retrograde Flow Past an Elliptic Cylinder

To conclude our series of numerical experiments, we consider the case of retrograde flow past an elliptic cylinder for inclinations of $\eta = 90°$ and $\eta = 15°$ (which corresponds to $\eta = -15°$ for the prograde case).

In Figure 17, $\eta = 90°$, $Re = 1000$ and $\hat{\beta} = 1$. No traveling Rossby waves are visible in the flow field. It is clear that the β-effect influences boundary-

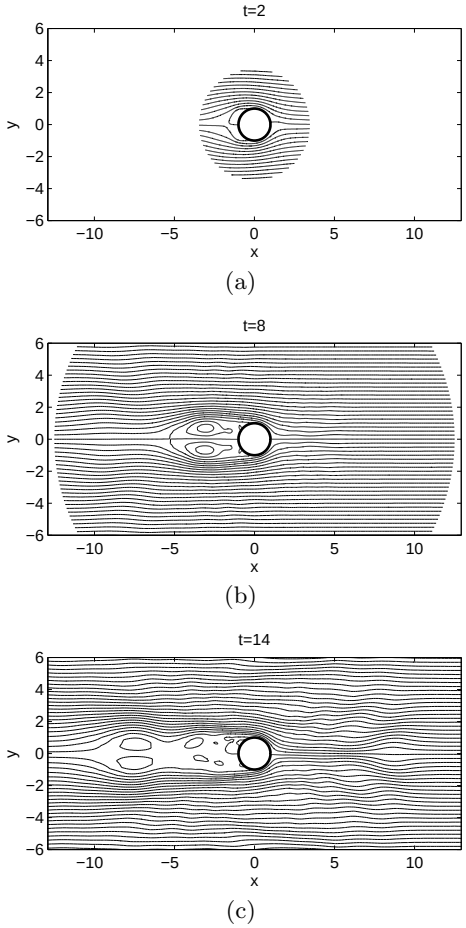

(a) (b) (c)

Fig. 13 Streamlines of perturbed retrograde flow past a circular cylinder for the parameters $Re = 1000$, $\hat{\beta} = 1$.

layer separation. The two initial recirculation vortices that form propagate downstream and are followed by a series of smaller-scale recirculation vortices. The separation region also grows to be much longer than in the non-rotating case. These results are indeed reminiscent of retrograde flow past a circular cylinder when $Re = 1000$ and $\hat{\beta} = 1$, with the exception that Rossby waves appear to be absent in the flow field.

Finally, in the case where $\eta = 15°$, $Re = 1000$ and $\hat{\beta} = 1$ (not shown), the results appeared much the same as in the non-rotating case (i.e. a reflected image of figure 15). Rossby waves were not visible in the flow field, and apart from timing the vortex shedding process appeared to continue as usual.

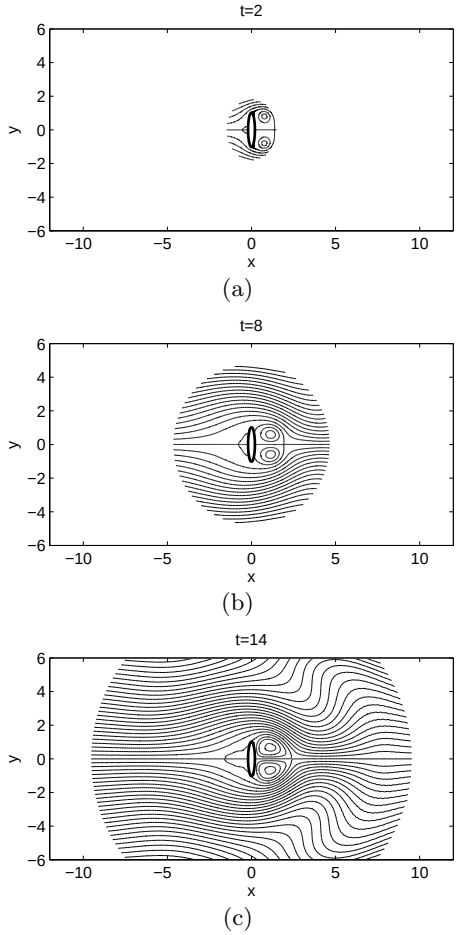

Fig. 14 Streamlines of prograde flow past an elliptic cylinder for the parameters $r = 0.2$, $\eta = 90^\circ$, $Re = 1000$, $\hat{\beta} = 1$.

6 Concluding Remarks

This paper revisited the problem of barotropic flow on the β-plane past cylindrical obstacles having circular and elliptic cross sections. The two non-dimensional parameters of interest are the Reynolds number, Re and the non-dimensional beta-parameter $\hat{\beta}$. To solve the problem on a large or unbounded domain with uniform far-field conditions, a modified β-plane approximation was proposed. An efficient numerical solution procedure for computing the flow field for small to moderately large Reynolds numbers was also presented. The focus of this investigation was on the early to moderate stages of the flow development following an impulsive startup. With this restriction on the

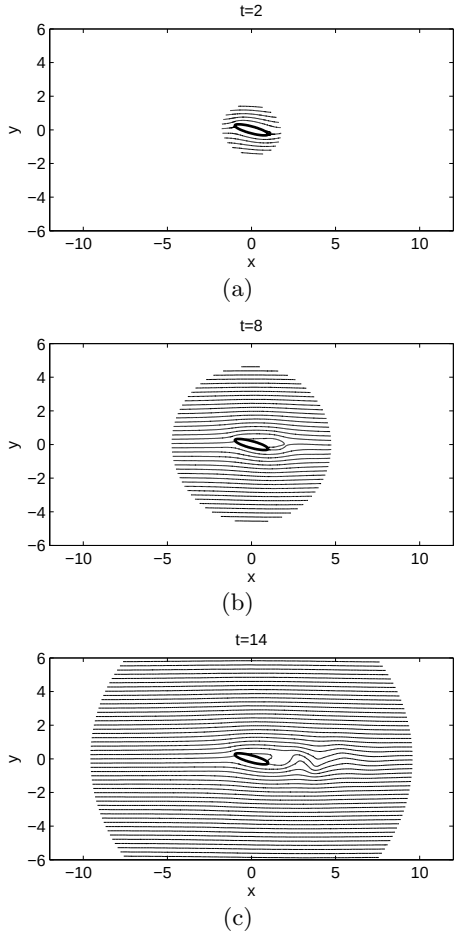

Fig. 15 Streamlines of prograde flow past an elliptic cylinder for the parameters $r = 0.2$, $\eta = -15°$, $Re = 1000$, $\hat{\beta} = 0$.

time interval, it is reasonable to assume that the flow will remain laminar and two-dimensional.

For prograde flow with $\hat{\beta} \leq 1$, our results concerning Rossby wave activity appeared to agree with those reported by [13], [18], and [8] despite the fact that their results assumed an inviscid ($Re \to \infty$) fluid.

While the results presented here for the case of viscous prograde flow past a circular cylinder are qualitatively similar to those reported by [16] for $\hat{\beta} \leq 1$, there is one subtle difference. In our simulations the flow remains symmetric unless it is perturbed while those in [16] are asymmetric.

When $\hat{\beta}$ was increased to $\hat{\beta} = 10$, our results indicated that a pair of strong western boundary currents formed at the shoulders of the cylinder which extended eastward along the cylinder's tiny separation region where

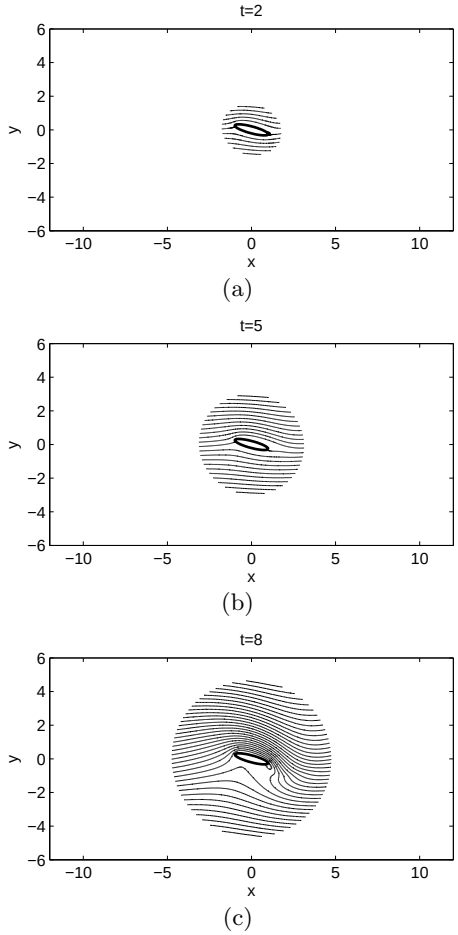

Fig. 16 Streamlines of prograde flow past an elliptic cylinder for the parameters $r = 0.2$, $\eta = -15^\circ$, $Re = 1000$, $\hat{\beta} = 0.75$.

they joined to form a single eastward zonal jet maintained by Rossby wave breaking on either side of the jet. [16] reported that these western boundary currents remained separated and extended downstream as a pair of zonal jets being maintained by breaking Rossby waves in the cylinder's turbulent separation wake.

Retrograde flow past a circular cylinder was found to possess some different features from prograde flow. These features appeared to agree with the experimental observations made by [3]. The main difference lies in the separated region which in retrograde flow becomes elongated. Additionally, standing Rossby waves cannot be generated as is explained by the dispersion relation for linear Rossby waves in a westward background flow.

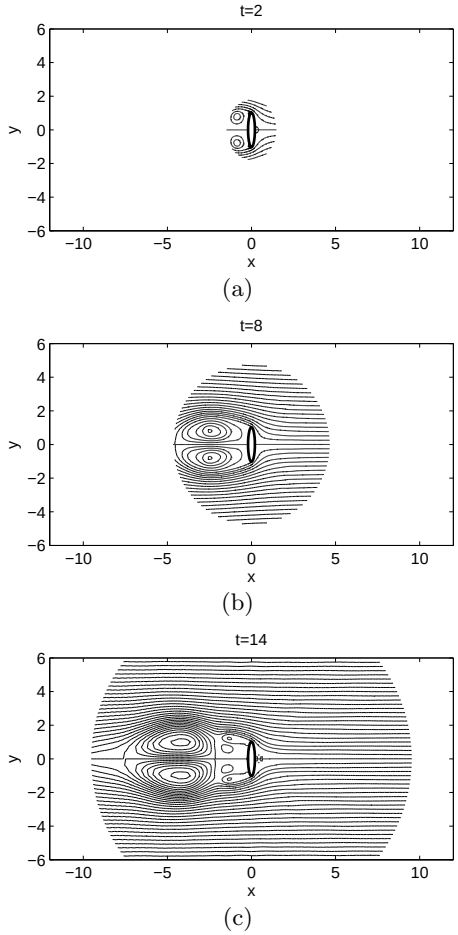

Fig. 17 Streamlines of retrograde flow past an elliptic cylinder for the parameters $r = 0.2$, $\eta = 90^\circ$, $Re = 1000$, $\hat{\beta} = 1$.

The β-effect posed similar constraints for the case of symmetric prograde flow past a slender elliptic cylinder. The case of retrograde flow, on the other hand, behaved in a similar fashion as perturbed flow past a circular cylinder for the same Re and $\hat{\beta}$. For asymmetric prograde flow past a slender elliptic cylinder vortex shedding shedding was suppressed for small to moderate times. Vortices were found to propagate around the trailing edge instead of in the expected downstream direction, as observed in the non-rotating case. For retrograde flow past an inclined elliptic cylinder, the β-effect appeared to have little or no influence on the structure of the flow.

Acknowledgements Financial support for this research was provided by the Natural Sciences and Engineering Research Council of Canada.

References

1. Badr, H., Dennis, S.: Time dependent viscous flow past an impulsively started rotating and translating circular cylinder. J. Fluid Mech. **158**, 447–488 (1985)
2. Badr, H., Dennis, S., Kocabiyik, S.: Numerical simulation of unsteady flow over an elliptic cylinder at different orientations. Internat. J. Numer. Methods Fluids **37**, 905–934 (2001)
3. Boyer, D., Davies, A.: Flow past a circular cylinder on a beta-plane. Phil. Trans. R. Soc. Lond. **A306**, 533–556 (1982)
4. Bryan, K.: A numerical investigation of a nonlinear model of a wind-driven ocean. J. Atmos. Sci. **20**, 594–606 (1963)
5. Dennis, S., Chang, G.Z.: Numerical solutions for steady flow past a circular cylinder at Reynolds numbers up to 100. J. Fluid. Mech. **42**, 471–489 (1970)
6. Dennis, S., Quartapelle, L.: Some uses of Green's theorem in solving the Navier-Stokes equations. Int. J. Numer. Meth. Fluids **9**, 871–890 (1989)
7. Dennis, S., Young, P.: Steady flow past an elliptic cylinder inclined to the stream. J. Eng. Math. **47**, 101–120 (2003)
8. Matsuura, T.: The separation of flow past a circular cylinder on a β-plane. J. Oceanogr. Soc. Japan **42**, 362–372 (1986)
9. McIntyre, M., Palmer, T.: Breaking planetary waves in the stratosphere. Nature **305**, 593–600 (1983)
10. Merkine, L.O.: Flow separation on a beta-plane. J. Fluid Mech. **99**, 399–409 (1980)
11. Oseen, C.: Übder die Stokes'sche formel, ünd uber eine verwandte aufgabe in der hydrodynamik. Ark Math. Astrom. Fys. **6**(29) (1910)
12. O'Sullivan, D., Hitchman, M.: Inertial instability and Rossby wave breaking in a numerical model. J. Atmos. Sci. **49**, 991–1002 (1992)
13. Page, M., Johnson, E.: Flow past cylindrical obstacles on a beta-plane. J. Fluid Mech. **221**, 349–382 (1990)
14. Rhines, P.: Waves and turbulence on a beta-plane. J. Fluid Mech. **69**, 417–433 (1975)
15. Steinmoeller, D., Flow separation on the β-plane, M.Math thesis, University of Waterloo, Waterloo, Ontario (2009)
16. Tansley, C., Marshall, D.: Flow past a cylinder on a β-plane, with application to Gulf Stream separation and the Antarctic Circumpolar Current. J. Phys. Oceanogr. **31**, 3274–3283 (2001)
17. Viúdez, A.: A New Interpretation of the Beta Term in the Vorticity Equation. J. Atmos. Sci. **60**, 1866–1870 (2003)
18. White, W.: A Rossby wake due to an island in an eastward current. J. Phys. Oceanogr. **1**, 161–168 (1971)